Title: Redefining Near-Unity Luminescence in Quantum Dots with Photothermal Threshold Quantum Yield

Authors: David A. Hanifi[2*], Noah D. Bronstein[1*], Brent A. Koscher[1,3*], Zach Nett[1], Joseph K. Swabeck[1,3], Kaori Takano[4], Adam M. Schwartzberg[7], Lorenzo Maserati[7§], Koen Vandewal[5], Yoeri van de Burgt[6], Alberto Salleo[2†], A. Paul Alivisatos[1,3,8‡]

Affiliations:

1. Materials Sciences Division, Lawrence Berkeley National Laboratory, Berkeley, CA 94720, USA.
2. Department of Materials Science and Engineering, Stanford University, Stanford, California, USA
3. Department of Chemistry and Department of Materials Science and Engineering, University of California, Berkeley, California 94720, USA
4. Materials R&D group, HPM Research & Development Dept, High Performance Materials Company, JXTG Nippon Oil & Energy Corporation, 8 Chidori-Cho, Naka-ku, Yokohama, Kanagawa, 231-0815, Japan
5. IMO-IMOMEC, vzw and Institute for Materials Research, Hasselt University, Wetenschapspark 1, 3590 Diepenbeek, Belgium
6. Microsystems, Institute for Complex Molecular Systems, Eindhoven University of Technology, 5612AJ Eindhoven, The Netherlands
7. The Molecular Foundry, Lawrence Berkeley National Laboratory, Berkeley, CA 94720, USA
8. Kavli Energy NanoScience Institute, Berkeley, CA 94720, United States

[*] These authors contributed equally to this work
[§]Present address: Center for Nano Science and Technology@PoliMi, Istituto Italiano di Tecnologia, 20133 Milano, Italy
[†] Corresponding author: asalleo@stanford.edu
[‡] Corresponding author: paul.alivisatos@berkeley.edu

Abstract: A variety of optical applications rely on the absorption and reemission of light. The quantum yield of this process often plays an essential role. When the quantum yield deviates from unity by significantly less than 1%, applications such as luminescent concentrators and optical refrigerators become possible. To evaluate such high performance, we develop a measurement technique for luminescence efficiency with sufficient accuracy below 1 part per thousand. Photothermal threshold quantum yield was developed utilizing the quantization of light to minimize overall measurement uncertainty. This technique is used to guide a procedure capable of making ensembles of near-unity emitting CdSe/CdS core/shell quantum dots. The photothermal threshold quantum yield luminescence efficiency reaches 0.996 ± 0.002, indicating nearly complete suppression of nonradiative decay channels.

One Sentence Summary: CdSe/CdS quantum dots synthesized and accurately measured with external luminescent efficiencies that exceed 99.5%

Main Text: Photoluminescence, the absorption and reemission of light, is an essential feature of numerous dyes and semiconducting materials. Recent commercial applications include solid-state lighting(*1*), high efficiency color displays, and bioimaging(*2*). Moreover, there are ongoing efforts to commercialize luminescent solar concentrators (LSCs)(*3*) and spectrum-shifting greenhouses(*4*). Each of these applications have specific performance requirements, which are assessed by a standard set of measurements techniques. An essential performance metric is the photoluminescence quantum yield (PLQY), which is determined by the competition between radiative relaxation of the excited material and non-radiative losses, typically due to defects. The PLQY is directly related to the electronic and structural quality of materials, with the highest values recorded to date of 99.7% and 99.5% respectively in rare-earth doped high-bandgap single crystals(*5*) and epitaxially-deposited thin films(*6*). However, in many commercial applications relying on photoluminescence, nanocrystals have important potential advantages over their molecular or bulk/thin film counterparts, which include stability, low cost, ability to be selectively placed inside a variety of composites, fluids, polymers, and biological environments, large-area processing compatibility and absorption/emission tuneability. The PLQY for CdSe/CdS, the prototypical core/shell quantum dot in research labs, routinely exceeds 95%(*7*). But this is insufficient for applications that require an absolute minimum amount of photon energy to be lost as heat. For example, the light concentration of LSCs increases logarithmically as the nonradiative losses of the luminophore vanish(*8*). Optical refrigeration(*9*), thermophotovoltaic engines(*10*), and thermal energy storage in optical cavities(*11, 12*) all require materials with PLQY $\geq$ 99% with negligible non-radiative losses(*13-15*).

Inspired by the photon recycling needs of LSCs(*13*), we aim here to reduce the reabsorption losses by keeping the single pass PLQY as high as possible while retaining a narrow emission linewidth. We achieve this through the growth of a 4 to 11 monolayer (ML) CdS shell around a highly monodisperse CdSe core. Our synthesis technique is inspired by the work of Chen et al.(*7*), with some noteworthy modifications (SM1-2). The most significant change is the complete lack of oleylamine, which Chen et al. use to keep a narrow size distribution. We omit amines, as they can aid in the desorption of the Z-type Cd(oleate)$_2$ surface ligand(*16*). This synthesis strategy helps maintain a high ligand surface coverage, reducing possible surface traps while preserving high radiative efficiency. The resulting PLQY, as measured in an integrating sphere, is plotted in Fig. 1A as a function of CdS shell thickness for different batches of quantum dots grown with similar sized cores (around 3.3 – 3.6 nm). For a particle with a 2 nm thick shell, the

PLQY consistently exceeds 90%±2%, and after 4 nm of shell is grown the PLQY tends to exceed 97%±3%. Figure 1B shows standard characterization of representative samples, including the absorbance spectra, the photoluminescence (PL) spectra, the photoluminescence excitation (PLE) spectra scaled to core absorbance, and transmission electron micrographs. The photoluminescence spectrum has a full-width-at-half-maximum of 28-32 nm for all shown batches of particles. Critical for LSCs, the Stokes ratio increases as the shell thickness increases(*17*), reaching values of around 100. The wavelength-dependent PLQY of each of these samples were measured in an integrating sphere (Fig 1C) and are indistinguishable within error regardless of excitation wavelength (100%±3% and 97%±3% for 8 and 10 monolayers respectively).

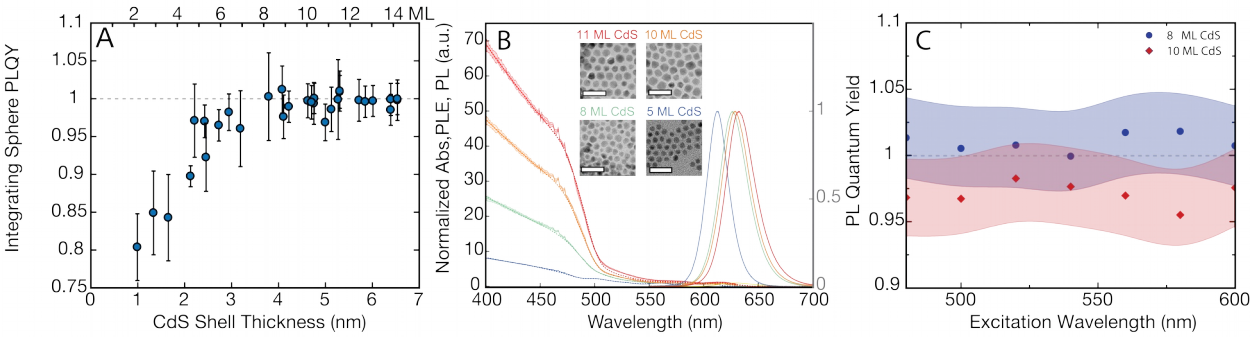

Fig. 1. Characterization of highly emissive CdSe/CdS quantum dots. (A) PLQY for many samples with different shell thicknesses grown with our synthesis procedure. (B) Absorption factor (dotted lines), PLE (shaded regions), and PL spectra (Solid lines) for 5, 8, 10, 11-monolayers CdS shells respectively. Inset: representative transmission electron micrographs, all scale bars are 25 nm. (C) Wavelength-resolved PLQY of 8 and 10-monolayer samples shown in figure 1B. Full characterization (SM4) dataset in figures S1-9.

Once the PLQY is within a couple of percent of unity, existing experimental measurements don't carry the accuracy necessary to provide feedback towards the materials' quality in order to further improve synthetic design. The most common and well characterized PLQY measurement techniques, the relative dye method and the integrating sphere technique, are both radiometry techniques at their core. Both rely on spectral sensitivity calibrations with a spectral radiance transfer standard, introducing at least 2% to 5% uncertainty into the measurement through the uncertainty of the spectral radiance transfer standard itself(*17, 18*).

In response to these optical sensitivity limitations, we developed a measurement of the PLQY that does not rely on photon flux measurement, but rather utilizes the quantization of light in a process analogous to the photoelectric effect. Instead of measuring the excitation energy threshold for electron emission, this technique measures the excitation energy threshold

that results in net positive heat generation. Therefore, we call our technique photothermal threshold quantum yield (PTQY).

In a typical photoluminescence event (Fig. 2A), an absorbed photon excites an electron from a ground state into a higher energy excited state leaving behind a hole; both charge carriers quickly (~picoseconds) relax to the band edges by emitting thermal phonons into the host crystal. At a later time (~nanoseconds), the thermalized electron and hole recombine bringing the material back to its ground state. This final transition can either be radiative or can be mediated by defects by emitting more heat, a non-radiative loss. Therefore, the average amount of heat emitted per absorption event is a combination of the intrinsic band-edge thermalization process (often called “blue loss” in the photovoltaic literature) and non-radiative band-to-band relaxation (“nonradiative loss”). Since the “blue loss” represents heat generated by carrier thermalization, an excitation energy dependent measurement of the heat per luminescence event allows us to determine the fraction of emitted heat that originates from nonradiative band-to-band relaxation. Determination of the photon energy at which the net emitted heat vanishes (E_0) allows us to precisely determine the PLQY (Fig 2B, SM6).

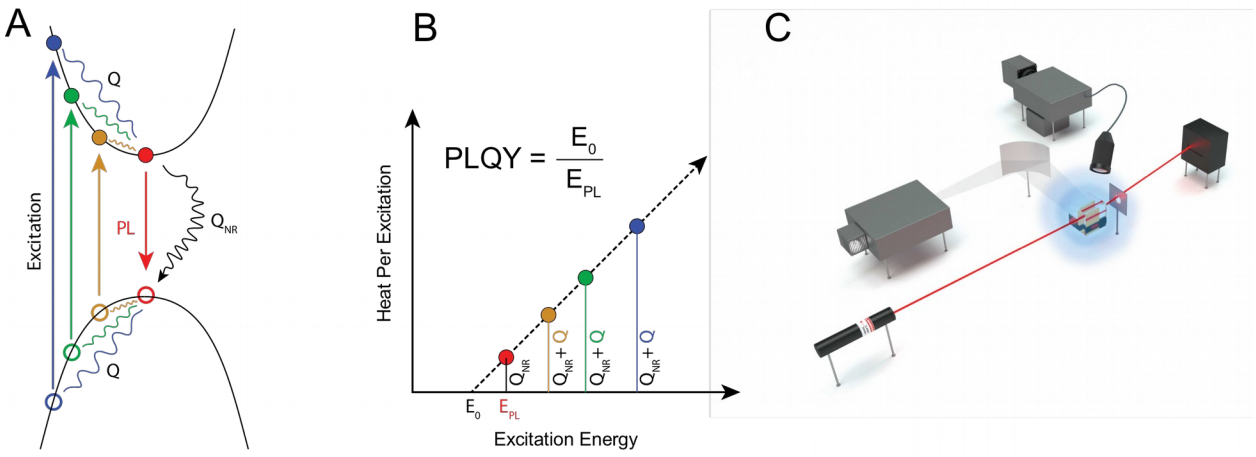

Fig. 2. Measurement scheme for the photothermal threshold quantum yield (PTQY) technique. (A) Excitation light is absorbed by an electron, which moves from a low energy state to a higher energy state. The excited electron and hole emit heat Q to relax to their lowest energy excited states, and then can recombine through photoluminescence or nonradiative processes (the latter of which emits heat Q_{NR}). (B) A plot of the heat emitted per excitation versus the excitation energy shows how the photoluminescence quantum yield (PLQY) can be determined from the threshold energy E_0 above which heat is emitted and the photoluminescence energy E_{PL}. A near perfect emitter at the thermal limit ($Q+Q_{nr}=0$) where the deviation of $E_{PL} \geq E_0$, represents the deviation in photothermal threshold quantum yield (i.e. PLQY ≤ 1). (C) The instrumental realization of the PTQY technique utilizes a photothermal deflection spectrometer to measure heat, synchronized to a photoluminescence spectrometer which determines both E_{PL} and the number of excitation events (SM5-6, figs. S17-25).

We implemented (Fig 2C and SM5) the PTQY technique using a transverse photothermal deflection spectrometer(*19*) to measure the non-radiative heat and a photoluminescence spectrometer to measure the above-gap PL excitation spectrum. By measuring the ratio of non-radiative to radiative emission components, this technique is able to remove the spectral radiance dependence in the PLQY measurement (Figs. S10-16). By extrapolating a thermal limit, the experimental technique solely relies on the measurement of photon energies (i.e. E_{exc} and E_{PL}), values that can be determined significantly more accurately than quantifying spectral radiance. A spectral radiance transfer standard is required only in order to determine the correct shape of the photoluminescence spectrum, bringing an uncertainty limit of 6 ppm (Fig. 3D). Our apparatus has an experimental uncertainty of 0.02%, limited by the detection spectrometer wavelength accuracy, which was used both to characterize the excitation lamp energy and average emission energies. Typical measurements are further limited by finite averaging, commonly achieving uncertainties of 0.1-0.2% (Fig. 3D), while the best achieved uncertainty was 0.04%. Our method has a 100x improvement in uncertainty compared to the 4% for relative and integrating sphere measurements (*18*). Measurement of heat generation can be performed very sensitively; even optically heterogenous thermally thin samples (¿50 μm) present little complication (SM3&7 and Figs. S26-33 for details ensuring measurement fidelity).

The sensitivity of PTQY enables us to investigate high-quality CdSe/CdS quantum dots where PLQY surpasses 90% (Fig. 1A and 3C). The highest PTQY value, shown in Fig 3A, is 99.6%±0.2%. This value was measured for excitations originating in the CdS shell of an 8.5ML ((3.6±0.2 nm diameter core and 3.7±0.3 nm thick shell) CdSe/CdS core/shell sample. This photoluminescence efficiency compares favorably with the internal radiative

efficiency estimated indirectly in well-passivated GaAs (99.7%±0.2% extrapolated from photon recycling(*6*)) and single-crystal Nd:$Y_3Al_5O_{12}$ (99.5% ±0.2% measured via laser cooling(*5*)). One sample, shown in Fig 3B, exhibited small radiative variations between the shell and core, barely discernible by traditional methods. In this sample (inset in Fig 3B) the PLQY of core excitations is 96.2±0.1%, while the PLQY when exciting the shell is 93.6%±0.2%. We ascribe this decrease to shell excitations naturally leading to more trapping and non-radiative processes (SM8 for further discussion).

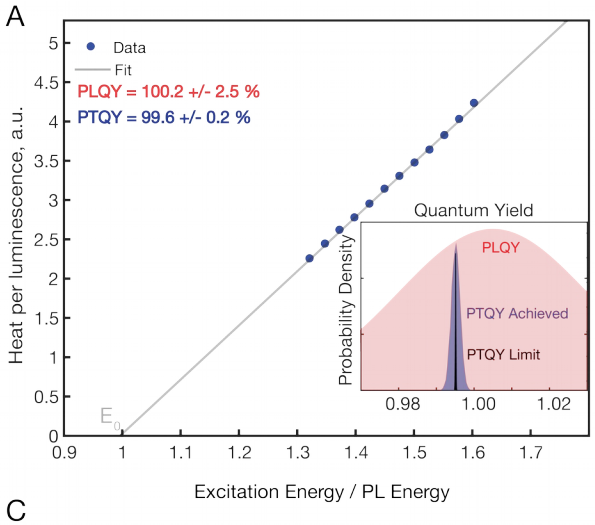

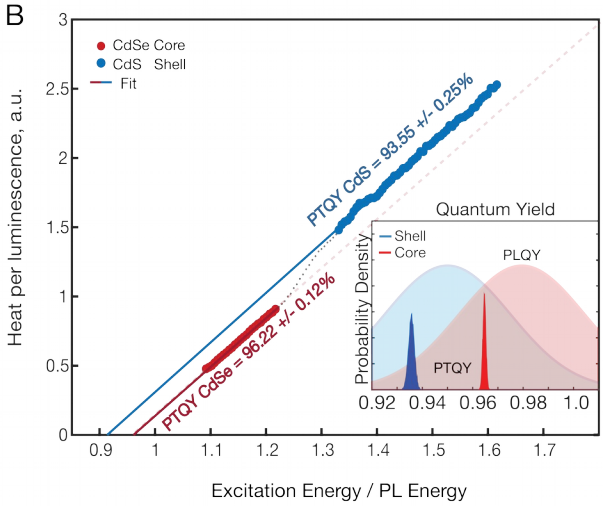

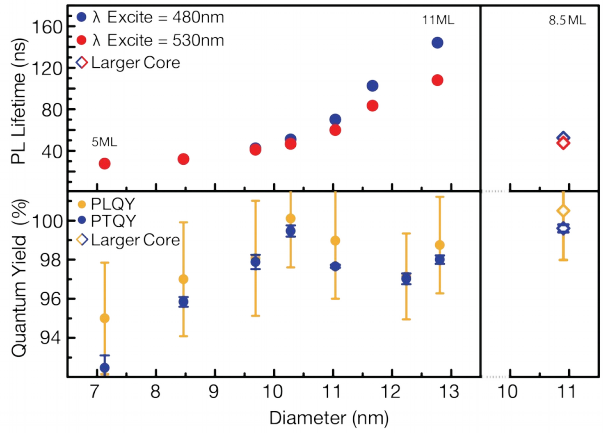

D

Sources of Uncertainty for PTQY measurement

Source of Uncertainty	Magnitude of Uncertainty	Uncertainty Contribution to PTQY
Finite Averaging	0.01% PDS 0.01% PL	0.00005
Wavelength Calibration of Detection Monochromator	0.02 nm	0.0002
Blackbody Irradiance Standard (Spectral Sensitivity Function of CCD)	2.5%	0.000006

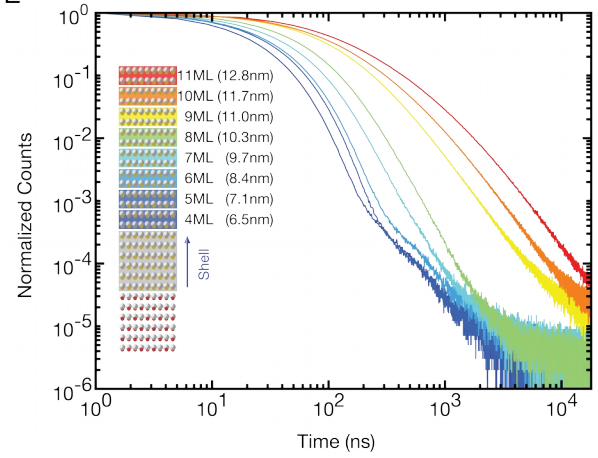

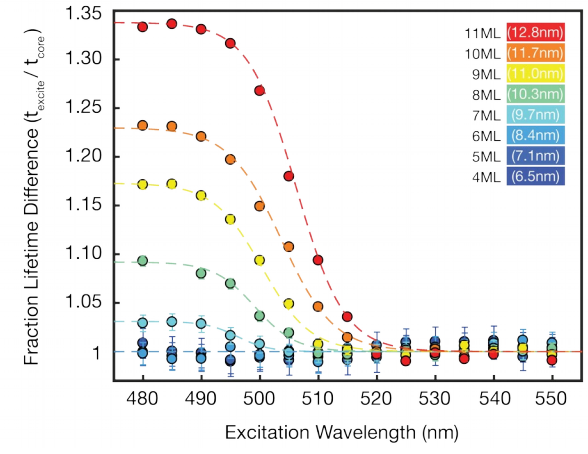

Fig. 3. Detailed optical characterization of CdSe/CdS quantum dots and PTQY measurement uncertainty. (A) PTQY of the best CdSe/CdS (core/shell) particles (8.5ML). The inset displays probability distributions and uncertainties associated with PTQY uncertainty, and integrating sphere PLQY (Gaussian), respectively. (B) High-resolution PTQY of high quality CdSe core (96.2 ±0.1%) but with poorly passivated CdS shell (93.6%±0.2) with inset of respective integrating sphere PLQY and PTQY uncertainty (Detailed uncertainty see SM6 & Figs. S10-16). (C) Top plot shows photoluminescence lifetimes of CdSe/CdS core and shell excited lifetimes and bottom plot shows respective PLQY and PTQY of the same near unity particles with measurement uncertainty plotted against particle Feret diameter, the circle markers represent a constant CdSe core size and varied CdS shell thickness, and the inset diamond markers represent the highest PTQY particles measured so far with a slightly larger 3.6±0.2 nm CdSe core and (8.5ML) 3.7±0.3 nm CdS shell. (D) Table representing the main sources of uncertainty and the general uncertainty budget for the calibrated PTQY spectrometer dependent on photon energy (Figs. S17-26). (E) TRPL data (log-log scale) taken at 407.1nm excitation. Despite near-unity PLQY of samples 4ML-11ML, significant differences in long lifetime components arise across the shelled series (F) Photoluminescence lifetime excitation wavelength dependence with varied shell thickness normalized to each particle's respective core lifetime.

We present a series of particles with the same size CdSe core but with different CdS shell thicknesses, 4 ML to 11 ML. We are able to systematically understand the origin of the peak in PLQY at 8 ML(±0.5ML), using PTQY and time-resolved PL decay (TRPL) measurements. With shell thicknesses less than 8ML, insufficient passivation consistent with surface hole traps is displayed(*20*), apparent in TRPL decays as a tail past ~100ns (Fig. 3E) resulting in significantly lower efficiencies (Fig. 3C). At and above 8 ML thick shells, the excited state decays are well-described by a bi-exponential decay, but above 8 ML, the excited state decays have substantially longer excited state lifetimes. The increasing excited state lifetime can be understood by considering the quasi-type II band alignment whereby a thicker shell results in reduced overlap between a delocalized electron in the shell and core-localized hole (SM8-9). Despite this extended lifetime, ensembles still display PTQYs of 99.6%, suggesting very slow nonradiative processes possibly as slow as 2-20 microseconds (Figs. S34-36). Moreover, excitations of larger shells allow the electron to be more easily trapped at the CdS surface in shallow traps (Fig. 3F). Thus core/shell particles can tolerate shallow surface traps that only affect one charge carrier(*21*). These results suggest an alternative, defect-tolerant path, towards the future development of quantum dots with 99.9% or better quantum yields, in addition to the well-known but challenging approach of eliminating all defects and trap levels in nanocrystalline samples which necessarily have an enormous surface area. The combination of more accurate PLQY measurements and increased TRPL

dynamic range, allows us to better track rare events that occur in quantum dot ensembles at excitation intensities single particle luminescence experiments can't achieve (Fig. S37). Such rare events under low flux excitation, $\langle N \rangle \ll 1$, where $\langle N \rangle$ is the average number of excitons created per pulse per particle, are relevant to further optimization of the particles for numerous energy related applications.

The true limit of colloidal quantum dot luminescence efficiency is currently not known. Improvements in both process engineering and luminescence efficiency quantification can help drive the design, synthesis, and understanding of optimized quantum dots, opening the door to tests of fundamental theory and applications of these important materials. In this work we have demonstrated a synthetic method that produces particles with external luminescent efficiencies that exceed 99.5%, and a measurement technique that is capable of measuring the efficiencies of these ensembles with nearly 100x less uncertainty than traditional measurement techniques. Our results demonstrate that there is no fundamental impediment to synthesize nanocrystals with non-radiative decay channels at least as low, if not lower, than those of the best single crystal semiconductor materials and provide an important platform for future development of near lossless materials at the thermodynamic limit.

References and Notes:

1. Y. Shirasaki, G. J. Supran, M. G. Bawendi, V. Bulović, Emergence of colloidal quantum-dot light-emitting technologies. *Nature Photonics* **7**, 13 (2012).
2. X. Michalet *et al.*, Quantum Dots for Live Cells, in Vivo Imaging, and Diagnostics. **307**, 538-544 (2005).
3. W. H. Weber, J. Lambe, Luminescent greenhouse collector for solar radiation. *Appl. Opt.* **15**, 2299-2300 (1976).
4. M. Hammam, M. K. El-Mansy, S. M. El-Bashir, M. G. El-Shaarawy, Performance evaluation of thin-film solar concentrators for greenhouse applications. *Desalination* **209**, 244-250 (2007).
5. T. Kushida, J. E. Geusic, Optical Refrigeration in Nd-Doped Yttrium Aluminum Garnet. *Phys. Rev. Lett.* **21**, 1172-1175 (1968).
6. I. Schnitzer, E. Yablonovitch, C. Caneau, T. J. Gmitter, Ultrahigh spontaneous emission quantum efficiency, 99.7% internally and 72% externally, from AlGaAs/GaAs/AlGaAs double heterostructures. *Appl. Phys. Lett.* **62**, 131-133 (1993).
7. O. Chen *et al.*, Compact high-quality CdSe–CdS core–shell nanocrystals with narrow emission linewidths and suppressed blinking. *Nature Materials* **12**, 445 (2013).

8. D. R. Needell *et al.*, Design Criteria for Micro-Optical Tandem Luminescent Solar Concentrators. *IEEE Journal of Photovoltaics* **8**, 1560-1567 (2018).
9. M. Sheik-Bahae, R. I. Epstein, Optical refrigeration. *Nature Photonics* **1**, 693 (2007).
10. R.M. Swanson, Recent developments in thermophotovoltaic conversion, International Electronic Device Meeting, Washington, DC, 1980. 10.1109/IEDM.1980.189789
11. T. Zhong *et al.*, Nanophotonic rare-earth quantum memory with optically controlled retrieval. *Science* **357**, 1392-1395 (2017).
12. T. P. Xiao, K. Chen, P. Santhanam, S. Fan, E. Yablonovitch, Electroluminescent refrigeration by ultra-efficient GaAs light-emitting diodes. *J. Appl. Phys.* **123**, 173104 (2018).
13. H.-J. Song *et al.*, Performance Limits of Luminescent Solar Concentrators Tested with Seed/Quantum-Well Quantum Dots in a Selective-Reflector-Based Optical Cavity. *Nano Lett.* **18**, 395-404 (2018).
14. D. A. Bender, J. G. Cederberg, C. Wang, M. Sheik-Bahae, Development of high quantum efficiency GaAs/GaInP double heterostructures for laser cooling. *Applied Physics Letters* **102**, 252102 (2013).
15. F. Meinardi *et al.*, Large-area luminescent solar concentrators based on 'Stokes-shift-engineered' nanocrystals in a mass-polymerized PMMA matrix. *Nature Photonics* **8**, 392 (2014).
16. N. C. Anderson, M. P. Hendricks, J. J. Choi, J. S. Owen, Ligand Exchange and the Stoichiometry of Metal Chalcogenide Nanocrystals: Spectroscopic Observation of Facile Metal-Carboxylate Displacement and Binding. *JACS* **135**, 18536-18548 (2013).
17. N. D. Bronstein *et al.*, Quantum Dot Luminescent Concentrator Cavity Exhibiting 30-fold Concentration. *ACS Photonics* **2**, 1576-1583 (2015).
18. C. Würth, M. Grabolle, J. Pauli, M. Spieles, U. Resch-Genger, Relative and absolute determination of fluorescence quantum yields of transparent samples. *Nature Protocols* **8**, 1535 (2013).
19. W. B. Jackson, N. M. Amer, A. C. Boccara, D. Fournier, Photothermal deflection spectroscopy and detection. *Appl. Opt.* **20**, 1333-1344 (1981).
20. M. Jones, S. S. Lo, G. D. Scholes, Quantitative modeling of the role of surface traps in CdSe/CdS/ZnS nanocrystal photoluminescence decay dynamics. *Proceedings of the National Academy of Sciences* **106**, 3011 (2009).
21. J. H. Olshansky, T. X. Ding, Y. V. Lee, S. R. Leone, A. P. Alivisatos, Hole Transfer from Photoexcited Quantum Dots: The Relationship between Driving Force and Rate. *JACS* **137**, 15567-15575 (2015).
22. J. Jasieniak, L. Smith, J. van Embden, P. Mulvaney, M. Califano, Re-examination of the Size-Dependent Absorption Properties of CdSe Quantum Dots. *The Journal of Physical Chemistry C* **113**, 19468-19474 (2009).

23. K. Vandewal *et al.*, Efficient charge generation by relaxed charge-transfer states at organic interfaces. *Nature Materials* **13**, 63 (2013).
24. K. Vandewal, L. Goris, K. Haenen, Y. Geerts, J. V. Manca, Highly sensitive spectroscopic characterization of inorganic and organic heterojunctions for solar cells. *Eur. Phys. J. Appl. Phys.* **36**, 281-283 (2006).
25. J. E. Sansonetti, W. C. Martin, Handbook of Basic Atomic Spectroscopic Data. *J. Phys. Chem. Ref. Data* **34**, 1559-2259 (2005).
26. F. T. Rabouw *et al.*, Temporary Charge Carrier Separation Dominates the Photoluminescence Decay Dynamics of Colloidal CdSe Nanoplatelets. *Nano Lett.* **16**, 2047-2053 (2016).
27. F. T. Rabouw *et al.*, Delayed Exciton Emission and Its Relation to Blinking in CdSe Quantum Dots. *Nano Lett.* **15**, 7718-7725 (2015).

Acknowledgments: The authors would like to thank Christopher J. Takacs, Victor Klimov, Warren Jackson, Rohit Prasanna, and Burak Guzelturk for their valuable advice, discussions or reading of the manuscript. **Funding:** This work is part of the 'Photonics at Thermodynamic Limits' Energy Frontier Research Center funded by the U.S. Department of Energy, Office of Science, Office of Basic Energy Sciences under Award Number DE-SC0019140. Work at the Molecular Foundry by A.M.S and L.M. (transient absorption measurements) was supported by the Office of Science, Office of Basic Energy Sciences, of the U.S. Department of Energy under Contract No. DE-AC02-05CH11231. Y.v.d.B (modeling and analysis) acknowledges funding from the European Research Council (ERC) under the European Union's Horizon 2020 research and innovation programme (grant agreement No. 802615). K.T. (synthesis methodology) acknowledges funding from JXTG Nippon Oil & Energy. **Author contributions:** D.A.H., N.D.B., and B.A.K., contributed equally to this work. D.A.H. and N.D.B. conceived the idea and directed the team. N.D.B., D.A.H., B.A.K., and Y.v.d.B. co-wrote the manuscript. D.A.H., N.D.B., Y.v.d.B., K.V. co-designed the PTQY experimental setup. B.A.K., N.D.B., and K.T. designed and developed the new synthetic method for CdSe/CdS nanoparticles used in this manuscript. B.A.K. and Z.N. synthesized the near unity nanocrystals used in this manuscript. D.AH., N.D.B., B.A.K., Z.N., J.S., A.M.S., L.M., and Y.v.d.B. all contributed to characterization of the samples in this paper. All authors contributed to the discussion and analysis of the results. **Competing interests:** Authors declare no competing interests. **Data and materials availability:** All processed data is available in the main text or in the supplementary materials. All software, and calibrations datasets, will be made available on the DASH repository https://doi.org/10.6078/D1XM30.

Supplementary Materials:

Science SI URL

Materials and Methods

Supplementary Text
Figs. S1 to S37
Tables S1 and S2
References (*22*-*27*)

5